Efficient ternary bulk heterojunction organic solar cells using a low-cost nonfullerene acceptor

Adrien Schlachter, Gabriel Marineau-Plante, Pierre Harvey, Anupam Agrawal, Ganesh Sharma

Efficient Ternary Bulk Heterojunction Organic Solar Cells Using A Low-cost Nonfullerene Acceptor

Adrien Schlachter,[1] Gabriel Marineau-Plante,[1] Pierre D. Harvey,[1]* Anupam Agrawal,[2] Ganesh D. Sharma,[2, 3]*

[1]Departement de chimie, Universite de Sherbrooke, Sherbrooke, PQ, Canada J1K 2R1

[2] Department of Physics, The LNM Institute of Information Technology, Jamdoli 302031 Jaipur, India

[3]Department of Electronics and Communication Engineering, The LNM Institute of Information Technology, Jamdoli 302031 Jaipur, India

Abstract

In order to improve the power conversion efficiency of single junction polymer solar cells (PSCs), we have used a ternary blend consisting of low bandgap D-A conjugated polymer **P** and two acceptors, *i.e*., one nonfullerene, **Cz-IC**, and one fullerene, $PC_{71}BM$. The concept of ternary bulk heterojunction (BHJ) using these two acceptors takes advantage of high electron mobility of the fullerene, which is beneficial for charge transport. The absorption spectra of $PC_{71}BM$, **Cz-IC** and **P** are complementary to each other, resulting in an increase in the light harvesting ability of the ternary BHJ active layer. The PSC based on an optimized ternary BHJ active layer attained a PCE of 15.27 %, which is higher than that of both binary PSCs based on **P**:$PC_{71}BM$ and **P**:**Cz-IC**. The increase in J_{SC} and FF for the ternary PSC with respect to the **P**:**Cz-IC** binary counterpart may be attributed to the better and balanced charge transport properties owing to the high electron mobility of $PC_{71}BM$. The incorporation of $PC_{71}BM$ in the **P**:**Cz-IC** blend also increases the hole transfer efficiency from both acceptors to **P**, thus reducing the charge recombination, resulting in a boost of the fill factor and overall PCE of the ternary OSC.

Key Words : A-D-A nonfullerene acceptor, ternary polymer solar cells, power conversion efficiency, solvent vapor annealing

*Corresponding authors : Pierre.Harvey@usherbrooke.ca (P. D. Harvey) and gdsharma273@gmail.com and gdsharma@lnmiit.ac.in (Ganesh D. Sharma)

Introduction

Over the last few years, particularly after 2015, with the aim of high efficiency bulk heterojunction polymer solar cells (BHJ-PSCs), the design of nonfullerene small molecule acceptors (NFSMAs) [1-8] as alternative electron acceptors in BHJ-PSC have been the subject of intense investigations. Indeed, using NFSMAs, the power conversion efficiency (PCE) has been increased to the range of 17-18 % for single junction-based PSCs [9-15]. It was already predicted that PSCs exhibiting PCEs up to 20 % could be achieved with high stability when appropriate polymer donors and NFSMAs were used in the BHJ active layer of PSCs [16, 17] and could possibly be candidates for future eco-friendly commercial applications [18-22].

Although remarkable PCEs have been reached for the binary BHJ PSCs, the photon harvesting properties of these devices are limited since most organic semiconducting materials generally exhibit relatively narrow absorption profiles with the full-width-at-half-maximum less than 150 nm, which restrict further improvements of the PCEs of these devices. To improve the photon harvesting ability of the active layer as much as possible, the concept of ternary PSCs have been established by combining either two electron donors and one acceptor or two electron acceptors and one donor with complementary absorption profiles into a single BHJ active layer [23-27]. The addition of a third component either as an electron donor or an acceptor in the active layer may provide sufficient photon harvesting ability, modulate the degree of phase separation and molecular arrangement, and may also form cascade energy levels for either energy or charge transfer which is generally known to boost the PCEs of ternary PSCs in the range of 17-18 % [28-34]. Upon evolution of BHJ-PSC designs, the combination of a fullerene and a nonfullerene acceptor leads to ternary systems, and altogether has led to higher PCEs owing to the high electron mobility of the fullerene derivatives compared to that of NFSMAs [35]. This beneficial situation stems from a favorable morphology manipulation [36, 37].

The NFSMAs are generally built upon a push-pull A-D-A motif, and more rarely A-D, where A and D are electron withdrawing and donating groups, respectively. Among the donating group, carbazole-containing residues have attracted significant attention [38-52]. Over the past two years, the molecular design of the carbazole-based NFSMAs has evolved and several examples are presented in Fig. 1 along with the reported PCEs of their BHJ-PSCs (optimized values). The most employed electron withdrawing groups are malononitrile derivatives, notably those containing

extra electron withdrawing hetero atoms such as fluorides. In overall, there is a sensitive increase in PCEs upon incorporating these atoms.

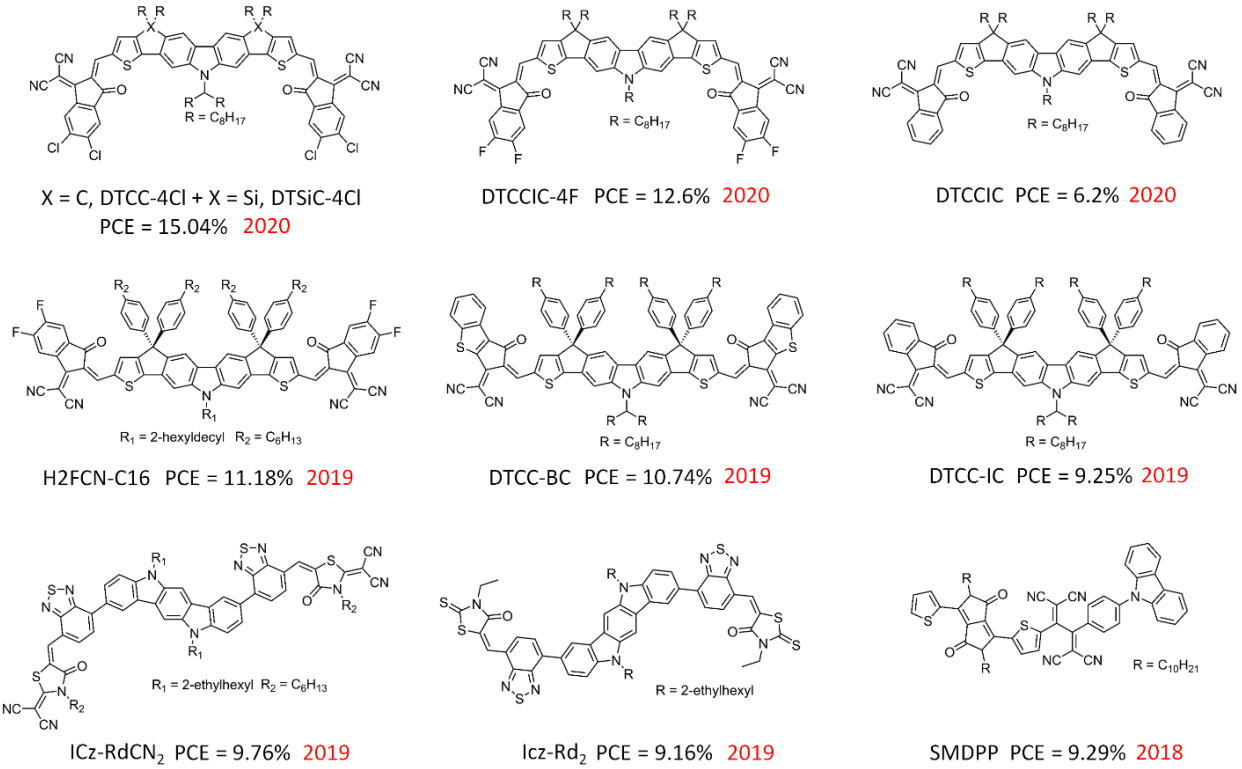

Fig. 1. Selected structures of recently reported carbazole-based NFSMAs along with their PCEs of their BHJ-PSCs (optimized values): DTCC-4Cl + DTSiC-4Cl (*i.e.* best PCE), [44], DTCCIC-4F [45], DTCCIC [45], DTCC-BC [46],DTCC-IC [46], H2FCN-C16 [47], ICz-Rd2, [48.49], ICz-RdCN2 [49], SMDPP [50]. This selection is based on the best ones where the carbazole residue is employed as a sub-fragment of the nonfullerene acceptor.

The simplest push-pull carbazole-containing dyads and triad are the mono- (**1**-**3**) and bis(malononitrile)carbazoles (**Cz-IC**) and their optical and electrochemical properties are known (**Fig. 2**) [53-56]. Moreover, compound **1** and **3** have been tested in organic solar cells of structure indium tin oxide (ITO)/MoOx (15 nm)/**1'** or **3** (15 or 30 nm)/C_{60} (50 nm)/bathocuproine (BCP, 6 nm)/Al (100 nm) [55]. Concurrently, compound **2** has been tested in a dye sensitized solar cell using a NiO electrode [56]. However, the resulting PCEs were found to be very modest (0.01 < PCE < 1.61%).

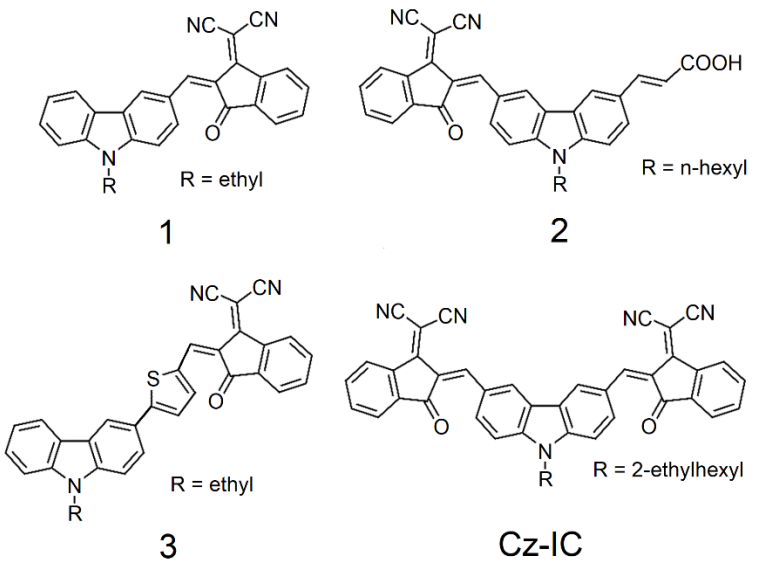

Fig. 2. Structures of **1** – **3** and **Cz-IC.**

We now report the photovoltaic properties of an ADA material denoted as **Cz-IC** employed as a NFSMA in ternary solar cells where $PC_{71}BM$ is used as a second electron acceptor. The low bandgap D-A conjugated polymer **P** composed of a 2,8-dibisthiophene-benzotrithiopne donor (D) unit and a fluorinated benzothiadiazole acceptor (A), linked *via* thiophene linker [57] is also incorporated inside the active layer of BHJ-PSCs in this investigation. The best PCE is found to be larger than 15.27%, which can be considered highly efficient, *i.e.* a record, even though no electron withdrawing atoms, such as fluorine, are introduced onto the skeleton of the molononitrile-containing groups. Because **Cz-IC** can be prepared in only four steps from commercial starting materials, instead of about 10 steps generally encountered in NFSMAs presented in **Fig. 1**, this carbazole-based ADA triad can be considered to be rather inexpensive.

Experimental section

Materials device fabrication and characterization

Cz-IC [54] was prepared from a literature method. The technique adopted for the fabrication organic solar cells and their characterization is described in Supporting Information (SI).

Results and discussion

Fig. 3a and **3b** exhibit the chemical structure and absorption spectra of **P**, **Cz-IC** and **$PC_{71}BM$**, respectively. The **P** donor absorbs between 550 and 900 nm, while the **Cz-IC** acceptor shows complementary absorption bands situated between 400 and 650 nm. $PC_{71}BM$ also absorbs

light below 600 nm where both **P** and **Cz-IC** exhibit weaker absorption features. Moreover, $PC_{71}BM$ exhibits high electron mobility and can be considered as an electron transport medium.

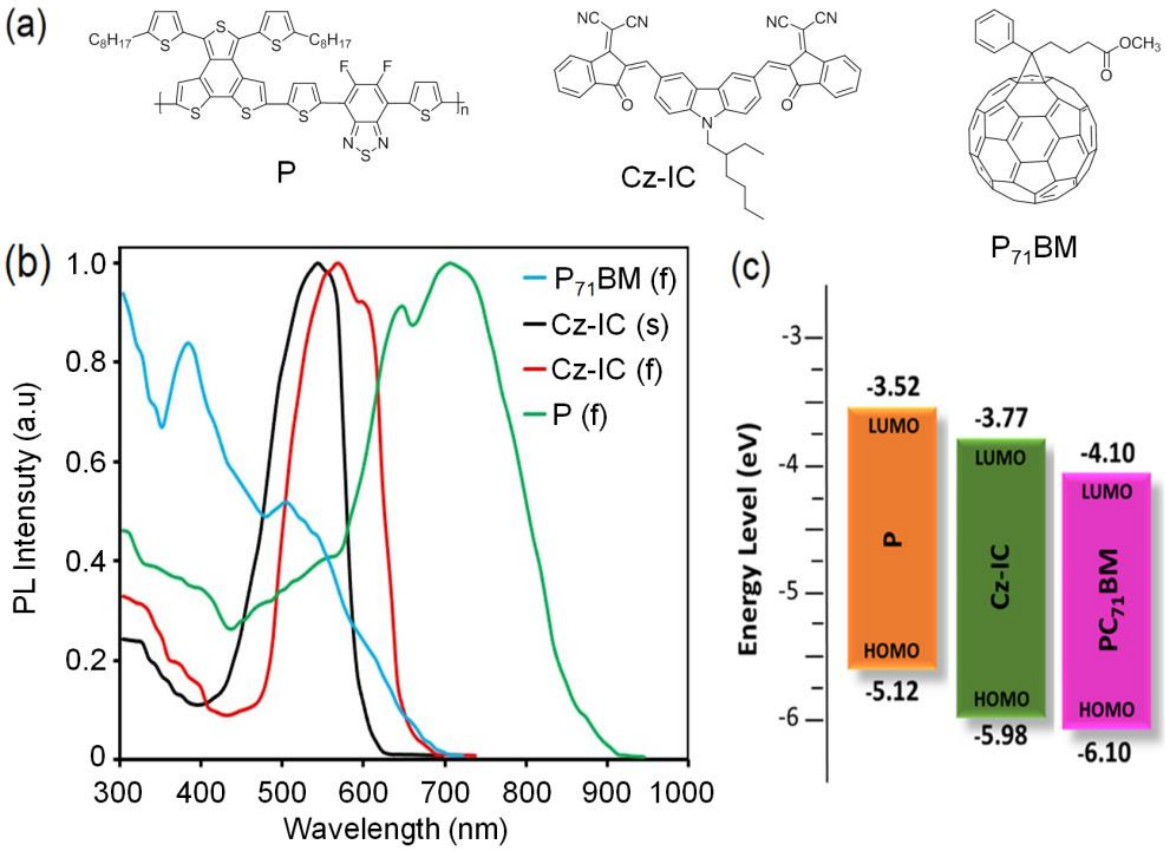

Fig. 3. (a) Chemical structure of **P**, **Cz-IC** and $PC_{71}BM$. (b) Absorption spectra of **Cz-IC** (s = solution), **Cz-IC** (f = film), and $PC_{71}BM$ and (c) energy band diagram of **P**, $PC_{71}BM$ and **Cz-IC**.

In BHJ-PSCs, after the exciton dissociation, the electron transfer (ET) from the donor to the acceptor and hole transfer (HT) from the acceptor to the donor are critical factors determining the overall PCE. The efficiency of the ET and HT is decided by both the lowest unoccupied molecular orbital (LUMO) and highest occupied molecular orbital (HOMO) energy offsets between the donor and the acceptor, respectively. Their energy level diagram of the materials is presented in **Fig. 3c**. The HOMO and LUMO energy levels are -5.12 /-3.52 eV for **P**, -5.98/-3.77 eV for **Cz-IC** and -6.10 /4.10 eV for $PC_{71}BM$. It can be seen from **Fig. 3c** that the HOMO offset between **P** and **Cz-IC** is high enough over the threshold value needed for exciton dissociation and subsequent hole transfer from the HOMO of **Cz-IC** to the HOMO of **P**. The LUMO offset between **P** and **Cz-IC** is about 0.16 eV, which is low enough for efficient electron transfer from the donor

to the acceptor used in the BHJ active layer of PSCs. To obtain information on the electron transfer from **P** to **Cz-IC**, the steady state photoluminescence spectra (PL) of the thin films for pristine **P** and **P**:**Cz-IC** blend excited at a wavelength near to the absorption peak of **P** have been measured (**Fig. 4**). The PL intensity of pristine **P** is significantly quenched by **Cz-IC** in the **P**:**Cz-IC** blended film. This PL quenching demonstrates the presence of an efficient photo-induced electron transfer from **P** to **Cz-IC** despite the modest LUMO offset between **P** and **Cz-IC**. Such a situation has already been reported in the literature for nonfullerene acceptor based BHJ-PSCs [58].

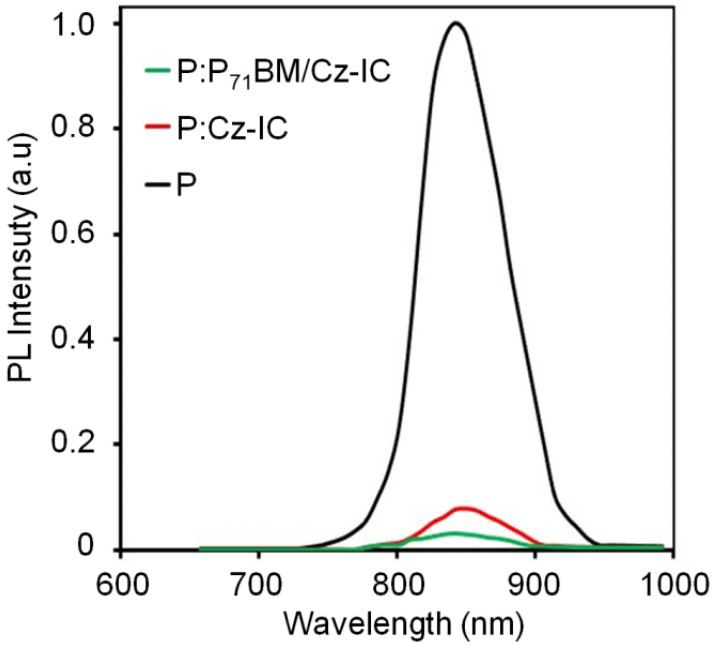

Fig. 4. Thin film PL spectra of pristine **P**, **P**:**Cz-IC** and **P**:P_{71}BM/**Cz-IC**

Single junction binary OSCs based on **P** donor and **Cz-IC** or $PC_{71}BM$ as acceptor were constructed with conventional indium tin oxide (ITO)/poly(3, 4-ethylenedioxythiophene) : poly-(styrenesulfonate) (PEDOT:PSS)/active layer/PFN/Al configuration. We have optimized the photovoltaic performance by varying the weight ratio between the donor **P** and acceptors ($PC_{71}BM$ or **Cz-IC**) using chloroform as processing solvent and found that the optimized ratios are 1:1.2 and 1:1.4 for **P**:**Cz-IC** and **P**:$PC_{71}BM$ BHJ active layers, respectively (the photovoltaic parameters are summarized in **Table S1a** and **S1b**). The optimized weight ratioed active layers were subjected to solvent annealing for 40s in THF vapor to further improve the photovoltaic performance. The total concentration for both active layers was 16 mg/mL. The fabrication details and procedure are described in the SI. The current-voltage (J-V) plots of the optimized OSCs under illumination

(AM1.5G, 100 mW/cm^2) are displayed in **Fig. 5a** and the related photovoltaic parameters are summarized in **Table 1**. The optimized OSCs based on **P**:$PC_{71}BM$ and **P**:**Cz-IC** showed a PCE of 8.99 % (V_{OC} of 0.74 V, J_{SC} of 17.88 mA/cm^2 and FF of 0.68) and 11.86 % (V_{OC} of 0.98 V, J_{SC} of 19.52 mA/cm^2 and FF of 0.62), respectively. The higher value of V_{OC} for **Cz-IC**-based OSCs compared to that of the $PC_{71}BM$ counterpart may be associated with the relatively upshifted LUMO energy level of **Cz-IC** as compared to $PC_{71}BM$ since the V_{OC} in the BHJOSC is directly related to the energy offset between the LUMO of the acceptor and HOMO of the donor [59]. The J_{SC} value for the **P**:**Cz-IC** -based PSC may be attributed to the broader absorption profile of the **P**:**Cz-IC** as compared to that for **P**:$PC_{71}BM$, since J_{SC} is linked to the light harvesting property of the BHJ active layer. The FF value of the **P**:$PC_{71}BM$-based PSC is larger than that of the **P**:Cz-IC-based counterpart, which may be associated with the superior electron mobility of fullerenes as compared to non-fullerene acceptors [60].

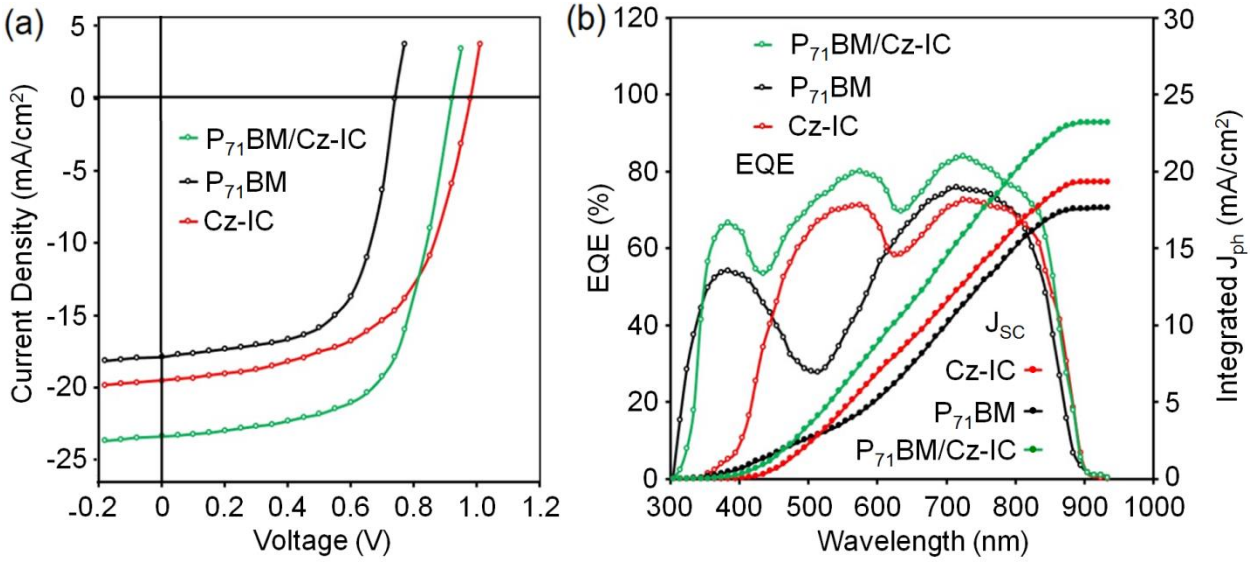

Fig. 5. Current-voltage (J-V) plots under illumination (AM1.5, 100 mW/cm^2) and (b) EQE and J_{SC} spectra for the optimized binary and ternary OSCs.

Considering the advantage of the high J_{SC} and V_{OC} values for binary **P**:**Cz-IC**-based PSCs, the high value of FF for the **P**:$PC_{71}BM$ counterpart, and the complementary absorption spectra of $PC_{71}BM$ and **Cz-IC**, a ternary BHJOSCs using **P** as electron donor and $PC_{71}BM$ and **Cz-IC** as acceptors has been fabricated. The photovoltaic performance of the ternary PSCs was optimized by varying the weight ratio between the two acceptors and kept the amount of donor **P** constant.

The **P**:$PC_{71}BM$/**Cz-IC** (1:0.2:1.0) PSC processed with CF solvent (total concentration 16 mg/mL) showed the best photovoltaic performance (detail is summarized in **Table S2**). The **P**:$PC_{71}BM$/**Cz-IC** active layer was also subjected to the SVA treatment as similarly performed for the binary active layers. The J-V curves for the optimized ternary PSC are shown in **Fig. 5a** and the photovoltaic parameters are summarized in **Table 1**. The optimized ternary PSC exhibits a PCE of 15.27 % (J_{SC}= 23.38 mA/cm^2, V_{OC} = 0.92 V and FF = 0.71), which is superior to that of the binary BHJ-PSCs. The larger value of J_{SC} of the ternary PSC is fully consistent with the fact that the PL intensity of **P** is more quenched in the **P**:$PC_{71}BM$/**Cz-IC** blend than that of the binary counterparts, indicating that the PET is more efficient in the ternary PSC as compared to the **P**:**Cz-IC** binary one.

Table 1. Photovoltaic parameters of the optimized binary and ternary PSCs.

Active layer	J_{SC} (mA/cm^2)	V_{OC} (V)	FF	PCE (%)	E_{loss}
P:$PC_{71}BM$	17.88 (17.63)[a]	0.74	0.68	8.99 (8.76)[a]	0.67
P:**Cz-IC**	19.52 (19.32)[a]	0.98	0.62	11.86 (11.72)[a]	0.42
P:$PC_{71}BM$/**Cz-IC**	23.38 (23.21)[a]	0.92	0.71	15.27 (15.04)[a]	0.48

a) Averaged values over eight identical devices.

In order to confirm the effect of the larger J_{SC} value in the ternary PSC as compared to the binary counterparts, the external quantum efficiency (EQE) of the PSCs was measured (**Fig. 5b**). The EQE response closely resembles that of the absorption spectra of the corresponding active layers (shown in **Fig. S1**, SI), thus demonstrating that all materials used in the active layers are contributing to the photocurrent generation. The broader EQE response of the ternary PSC may be attributed to fact that the light harvesting efficiency has increased for the ternary based OSC as compared to the binary counterparts [61, 62]. The J_{SC} spectra of the PSCs are also shown in **Fig. 5b**. The integrated values of J_{SC} are about 17.63, 19.32 and 23.21 mA/cm^2 for the optimized **P**:$PC_{71}BM$, **P**:**Cz-IC** and **P**:$PC_{71}BM$/**Cz-IC** based PSCs, respectively, and are very close to the values observed in the J-V data.

The V_{OC} value of the ternary PSC (0.92 V) is found to be in between the values observed for **P**:$PC_{71}BM$ (0.84 V) and **P**:**Cz-IC** (0.98 V). This outcome may be attributed to the alloy formation between the two acceptors. The HOMO and LUMO energy levels of $PC_{71}BM$/**Cz-IC** have been determined using CV measurements with different weight ratios between these two

acceptors and compiled in Table S4 (SI). The values of the HOMO and LUMO energy levels of the optimized blend are -6.02 and -3.88 eV, respectively. The LUMO energy level of the mixed acceptor ternary system lies between that of $PC_{71}BM$ and **Cz-IC**, which is consistent with the larger V_{OC} value found for binary PSCs based on **P**:$PC_{71}BM$ and lower V_{OC} value observed for the **P**:**Cz-IC** counterpart. In conclusion, the two acceptors, $PC_{71}BM$ and **Cz-IC**, form an alloy in the ternary BHJ active layer as reported in the literature [63, 64].

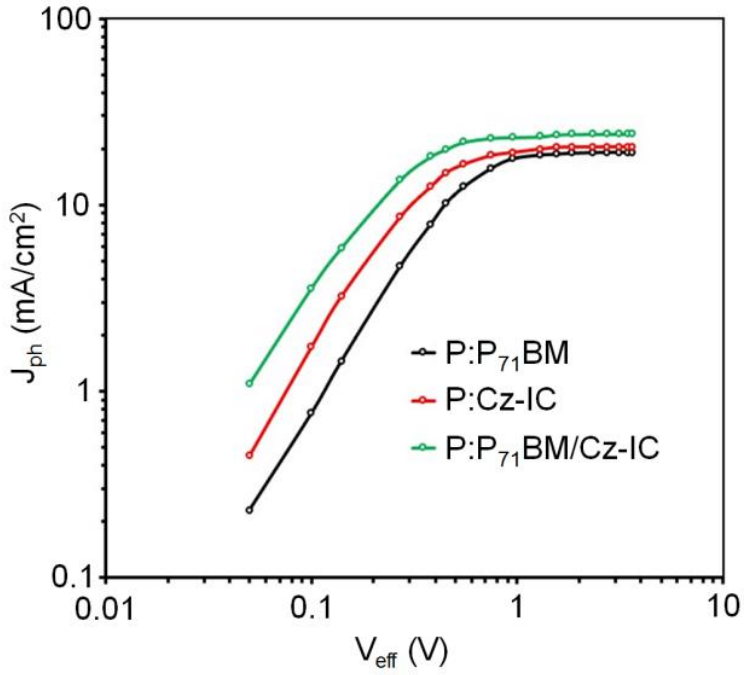

Fig. 6. Variation of the photocurrent density (J_{ph}) with the effective voltage (V_{eff}) for the optimized binary and ternary OSCs.

The photocurrent and FF values of the PSCs are known to depend on the exciton generation rate and their subsequent dissociation into free charge carriers and charge transports as well as their collection at their respective electrodes, *i.e.* holes at the anode and electrons at the cathode. In order to get information about the exciton generation rate (G_{max}), exciton dissociation rate and charge collection rate, the variation of photocurrent density (J_{ph}) as a function of effective voltage (V_{eff}) for these optimized PSCs have been examined [65,66] (**Fig. 6**). J_{ph} is described as $Jph = J_L - J_D$, where J_L and J_D are the current densities under illumination and in the dark, respectively. V_{eff} is expressed by $V_{eff} = V_o - V$, where V_o is the voltage at which $J_L = J_D$, and V is the applied voltage. After an initial increase in the J_{ph} with the increase in V_{eff}, the J_{ph} tends to saturate and finally

reaches the saturation current (J_{sat}) at V_{eff} > 1.2 V for all the investigated devices. The trend for J_{ph} follows this order: **P**:**Cz-IC** > **P**:$PC_{71}BM$ > **P**:$PC_{71}BM$/**Cz-IC**. The exciton dissociation (P_{diss}) and charge collection probability (P_{coll}) were estimated from J_{ph}/J_{sat} under short circuit and maximum power point conditions, respectively, and are summarized in **Table 2**. Both P_{diss} and P_{coll} are larger for the ternary PSC as compared to the binary counterparts, indicating that the exciton dissociation and charge collection are superior for the ternary PSC as compared to the binary counterparts. The G_{max} is also estimated using the expression $J_{max} = J_{sat}/qL$, where L is the thickness of the active layer and q is elementary charge. The G_{max} values for the PSCs are compiled in **Table 2**. The G_{max} of the ternary PSC is larger than that of the binary counterparts demonstrating that the light harvesting efficiency of the ternary BHJ is better than that of binary counterparts. This conclusion is validated by the EQE spectra of the binary and ternary PSCs. The J_{SC} value of the ternary OSCs is larger than that of the binary counterparts.

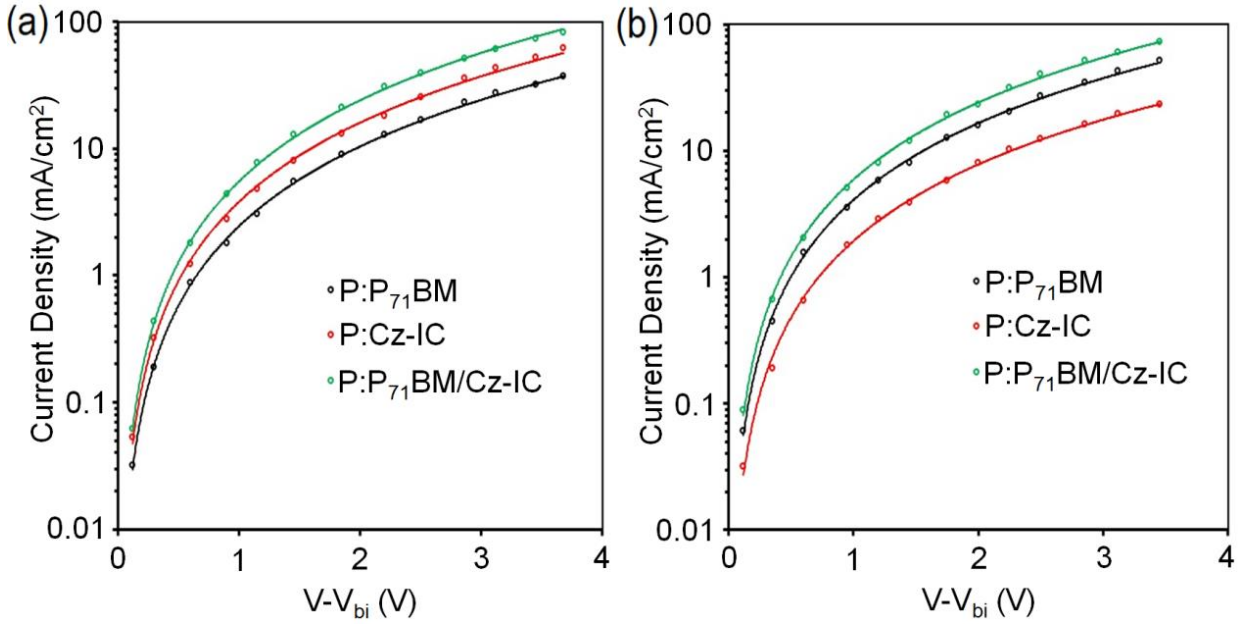

Fig. 7. Dark J-V curves with SCLC fitting for (a) hole only and (b) electron only devices for optimized binary and ternary active layers.

In order to provide understanding on the charge transport in the binary and ternary devices, the hole (μ_h) and electron (μ_e) mobilities have been measured from the dark J-V characteristics of *hole only* and *electron only* devices, respectively, and fitting the data with a space charge limited current (SCLC) model (**Fig. 7**). The data are compiled in **Table 2**. The μ_h and μ_e values of the

P:**Cz-IC** blend film are 3.46×10^{-4} and 1.38×10^{-4} cm^2/Vs, with corresponding μ_h/μ_e ratio of 2.51. When $PC_{71}BM$ is incorporated into the **P**:**Cz-IC** blend as a third component with a weight ratio of 1:0.3:0.9 (*i.e.* **P**: $PC_{71}BM$/**Cz-IC**), μ_h and μ_e increase up to 3.6×10^{-4} and 2.95×10^{-4} cm^2/Vs, respectively, resulting in a corresponding μ_h/μ_e ratio of 1.24. The larger charge carrier mobilities and more balanced μ_h/μ_e ratio for the ternary blend film may be attributed to the larger electron mobility of $PC_{71}BM$ phase, thus contributing to the superior values of both FF and J_{SC}, which ultimately resulted in an improvement in the overall PCE of the ternary OSC.

Table 2. Exciton generation rate, exciton dissociation, charge collection and mobility data for the devices.

Active layer	P_{diss}	P_{coll}	G_{max} ($m^{-3}s^{-1}$)	μ_h (cm^2/Vs)	μ_e (cm^2/Vs)	μ_h/μ_e
P:$PC_{71}BM$	0.937	0.81	1.23×10^{28}	2.21×10^{-4}	2.54×10^{-4}	0.87
P:**Cz-IC**	0.952	0.78	1.34×10^{28}	3.46×10^{-4}	1.38×10^{-4}	2.51
P:$PC_{71}BM$/**Cz-IC**	0.976	0.83	1.57×10^{28}	3.69×10^{-4}	2.95×10^{-4}	1.24

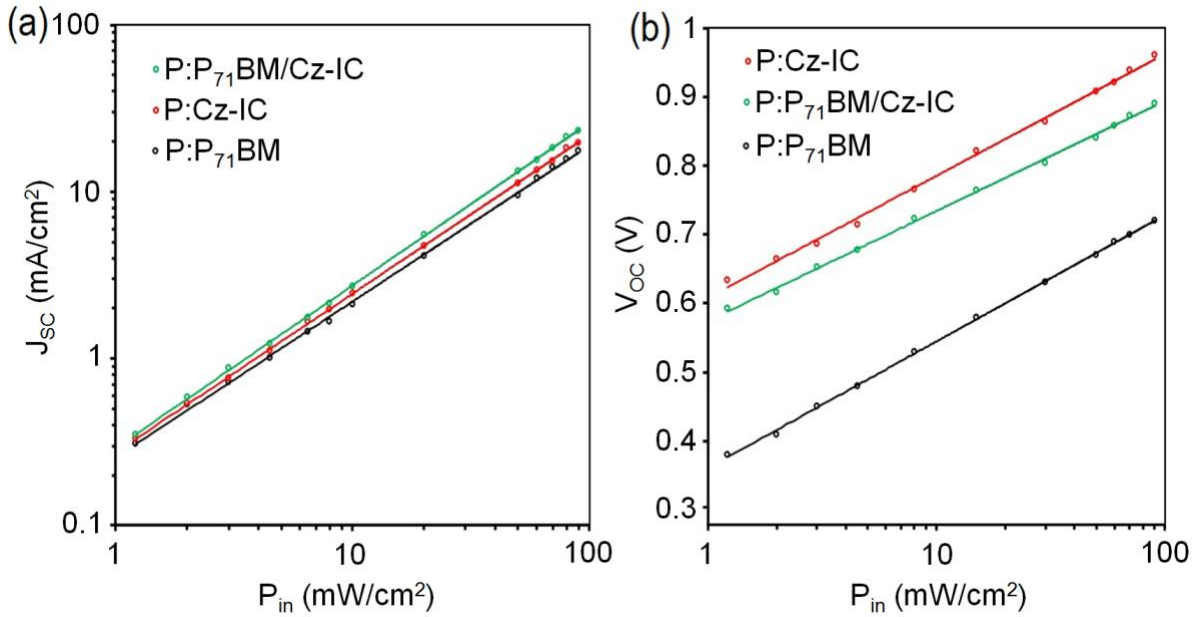

Fig. 8. Variation of (a) J_{SC} and (b) V_{OC} with illumination intensity (P_{in}) for the OSCs based on optimized binary and ternary PSCs.

The bimolecular charge recombination process in the PSCs was investigated by the analysis of J_{SC} *vs.* P_{in} (**Fig. 8a**). The dependance of J_{SC} with P_{in} follows the power law as described by $J_{SC} \propto (P_{in})^{\alpha}$, where α is an exponential factor, which provide information on the degree of bimolecular

recombination [67,68]. The α values estimated from **Fig. 8a** are 0.931, 0.945 and 0.974 for **P**:**Cz-IC**, **P**:$PC_{71}BM$ and **P**:$PC_{71}BM$/**Cz-IC**, respectively. The α value is larger and closer to unity for the ternary OSCs meaning that the bimolecular recombination is reduced by the incorporation of $PC_{71}BM$ in the **P**:**Cz-IC** binary blend. The variation of V_{OC} with P_{in} is shown in **Fig. 8b** and the dependance follows the expression $V_{OC} \propto n(KT/q) \ln (P_{in})$, where K, T and q are the Boltzmann's constant, absolute temperature, and elementary charge, respectively. In general, the 'n' value lies in between 1 and 2. When 'n' is close to 1, the losses of charges are due to the bimolecular recombination whereas when n is close to 2, the charge loss is due to trap-assisted recombination. The fitted n values for **P**:$PC_{71}BM$ binary, **P**:**Cz-IC** binary and **P**:$PC_{71}BM$/**Cz-IC** ternary OSCs are 1.26, 1.32 and 1.15, respectively. The lowest 'n' value for the ternary OSC indicates that the trap-assisted recombination also reduced in the ternary active layer.

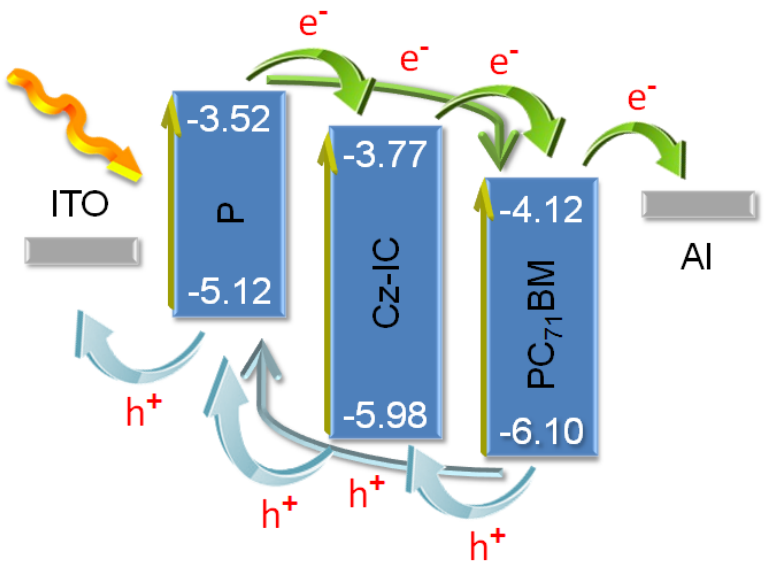

Fig. 9. Charge and hole transfer mechanisms in the ternary BHJ active layer-based PSCs.

In order to get information about the charge transfer between the two acceptors, the J-V characteristics of the devices under illumination using pristine PC71BM, **Cz-IC** and optimized **Cz-IC**:$PC_{71}BM$ blend as active layer have been measured and the data are shown in **Fig. S2** (SI). The J_{SC} of the device based on **Cz-IC**:$PC_{71}BM$ is about 3.86 mA/cm^2, which is larger than that of either $PC_{71}BM$ (0.98 mA/cm^2) and **Cz-IC** (1.78 mA/cm^2), indicating that there is a photo-induced charge transfer between two acceptors. As the LUMO energy offsets (0.35 eV) between $PC_{71}BM$ and **Cz-IC** is sufficiently higher than that of the driving force needed for the ET from **Cz-IC** to

$PC_{71}BM$. We assume that the efficient ET is taking place in the acceptor blend. However, the HOMO energy offset (0.12 eV), which is significantly smaller than the threshold value of driving force needed for HT from the HOMO of $PC_{71}BM$ to the HOMO of **Cz-IC**. Therefore, the PL spectra of the pristine $PC_{71}BM$ and its blend with **Cz-IC** were recorded and are shown in **Fig. S3** (SI). The PL intensity of $PC_{71}BM$ is quenched in the $PC_{71}BM$:**Cz-IC** blend indicating that there is a PHT from $PC_{71}BM$. The possible charge and hole transfer mechanisms in the ternary BHJ OSCs are shown in **Fig. 9**. After generation of photoinduced excitons, the electrons from the HOMO of both acceptors are transferred to the HOMO of **P** and the electrons from the LUMO of **P** are transferred to both acceptors [69, 70].

The energy loss (E_{loss}) in the PSCs is estimated from $E_{loss} = E_{gopt} - qV_{OC}$, where E_{gopt} is calculated from the onset of the EQE spectra of the devices [71, 72]. The values of the E_{loss} are listed in **Table 1**. The E_{loss} for the ternary PSC is larger than that of the **P**:**Cz-IC** and smaller than that of the **P**:$PC_{71}BM$ based devices, which is consistent with the values of V_{OC} observed in the PSCs.

The morphology of the binary and ternary films was investigated by transmission electron microscopy (TEM) images and are shown in **Fig. 10**. The TEM images shows the dark and bright regions, which respectively correspond to the acceptor rich and electron rich areas due to their different electron densities. The **P**:**Cz-IC** and **P**:$PC_{71}BM$ showed apparent aggregation. The ternary active layer film aggregation is slightly improved, and the domain distribution is more continuous and uniform, which is beneficial for the formation of good interpenetrating network and phase separation for charge transport. It also provides more D/A interfaces and forms effective charge transport pathways, which leads to a significant improvement in the FF and PCE of the ternary PSCs [73]. The larger phase separation in the range of 20-25 nm between the donor and acceptor resulted in a suppression of charge recombination.

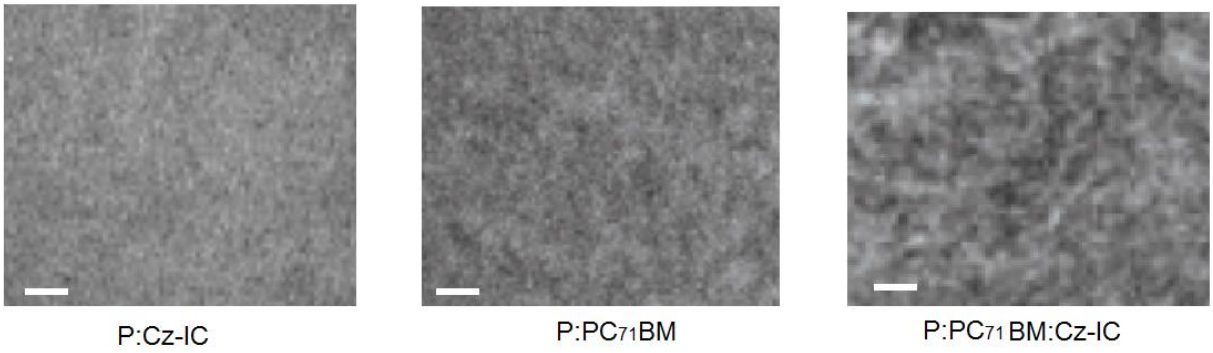

Fig. 10. TEM images of **P**:**Cz-IC**, **P**:$PC_{71}BM$ and **P**:$PC_{71}BM$/**Cz-IC** thin films. Scale bar is 100 nm

The effect of the incorporation of $PC_{71}BM$ into the **P**:**Cz-IC** on the molecular packing crystallinity of the active layer was investigated by X-ray diffraction (XRD) patterns, which are shown in **Fig. 11**. The parameters, *i.e.* d-spacing, π-π stacking distance and crystal coherence length (CCL) estimated from the XRD patterns are compiled in Table 3. The binary film exhibits the (100) ($2\theta = 4.79°$) and (010) ($2\theta = 23.79°$) diffraction peaks and corresponds to the lamellar diffraction and π-π stacking, respectively. Since the diffraction peaks of both **P** and **Cz-IC** overlap, it is not possible to distinguish their peaks in the binary and ternary blends. Upon incorporation of $PC_{71}BM$, the (100) and (010) peaks shift to 5.04° and 24.14°, respectively, and a new weak and broad signal appears at $2\theta = 18.23°$ corresponding to the $PC_{71}BM$ phase. The intensity of both (100) and (010) diffraction peaks for the ternary are stronger than that of the binary counterpart, indicating that the molecular ordering and crystallinity has increased with the addition of a small quantity of $PC_{71}BM$. The CCLs of both lamellar and π-π stacking for the ternary active film is larger than that of the binary counterpart, which is consistent with the phase separation observed in the TEM images. Moreover, the π-π stacking distance is shorter in the ternary films than that of the binary counterpart, which is beneficial for the charge transport, which suppresses recombination as observed by the mobility measurements. These observations are fully consistent with the larger FF value for the ternary PSCs as compared to the binary counterpart.

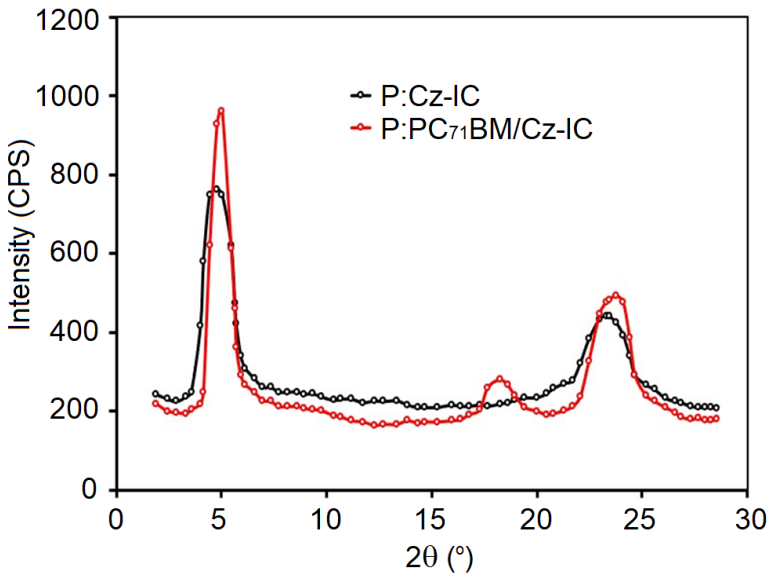

Fig. 11. XRD patterns for the binary and ternary films of **P**:**Cz-IC** and **P**:$PC_{71}BM$/**Cz-IC**.

Table 3. d-spacing and crystal coherence lengths for (100) and (010) diffraction peaks for **P**:**Cz-IC** binary and **P**:$PC_{71}BM$/**Cz-IC** ternary films.

Active layers	(100) peak		(010)	
	d-spacing (nm)	CCL (nm)	π-π stacking distance (nm)	CCL (nm)
P:**Cz-IC**	1.78	5.32	0.373	3.17
P:$PC_{71}BM$/**Cz-IC**	1.74	7.58	0.368	4.12

Conclusion

To the best of our knowledge, the simple A-D-A nonfullerene **Cz-IC** has been used in a PSC for the first time. Indeed, it was used for the fabrication of binary BHJ-PSCs using a narrow bandgap D-A polymer **P**. It proved to be a better electron acceptor than $PC_{71}BM$ in the binary active layers of the OSCs (*i.e.* **P**:**Cz-IC** and **P**:$PC_{71}BM$; respectively PCE = 11.86 and 8.99 %), which showed a high V_{OC} of 0.98 V with a J_{SC} value of 19.52 mA/cm^2. The high value of V_{OC} is attributed to the high lying LUMO of **Cz-IC**. Taking advantage of the high value of FF of 0.68 for **P**:$PC_{71}BM$ PSCs and high values V_{OC} and J_{SC} for the **P**:**Cz-IC**, we have fabricated ternary PSCs

based on **P**:$PC_{71}BM$/**Cz-IC** and after the optimization, the PSC showed an overall PCE of 15.27 % with energy loss of 0.48 eV. The increase in the PCE for the ternary PSC is mainly due to the increase in the J_{SC} and FF, and may be attributed to the formation of cascaded energy level in the ternary active layer, reduced π-π stacking distance and appropriate *phase* separation for charge transport and reduced charge recombination. In summary, **Cz-IC** can be prepared in only four steps, which makes this inexpensive underexploited nonfullerene molecule highly attractive. In the ternary system, **P**:**Cz-IC**/$PC_{71}BM$, the PCE increased to 15.27%, which places this value among the best OSCs, if not the best (**Table 1**), where the nonfullerene acceptor bears a carbazole sub-unit.

ACKNOWLEDGMENTS

This work was supported by the Natural Sciences and Engineering Research Council of Canada, the Fonds de Recherche du Qu bec-Nature et Technologies, Compute Canada and Calcul Qu bec, the Centre Quebecois sur les Mat riaux Fonctionnels.

Supporting Information

Device fabrication and characterization and photovoltaic parameters of the as cast **P**:$PC_{71}BM$, **P**:**Cz-IC**, and **P**:$PC_{71}BM$/Cz-IC based OSCs with different weight ratios between **P**, **Cz-IC** and $PC_{71}BM$.

References

1. G. Sauve, R. Fernando. Beyond fullerenes: designing alternative molecular electron acceptors for solution processable bulk heterojunction organic photovoltaics, J. Phys. Chem. Lett. 6 (2015), 3779-3780.
2. J. Hou, O. Inganas, R. H. Friend, F. Gao, Organic solar cells based on non-fullerene acceptors, Nat. Mater. 17 (2018) 119-128.
3. G. Zhang, J. Zhao, P.C. Y. Chow, K. Jiang, J. Zhang, Z. Zhu, J. Zhang, F. Huang, H. Yan, Nonfullerene acceptor molecules for bulk heterojunction organic solar cells, Chem. Rev. 118 (2018) 3447-3507.
4. A. Armin, W. Li, O. J. Sandberg, Z. Xiao, L. Ding, J. Nelson, D. Neher, K. Vandewal, S. Shoaee, T. Wang, H. Ade, T. Hewmuller, C. Brabec, P. Mersdith, A history and perspective

on non-fullerene electron acceptors for organic solar cells, Adv. Energy Mater. 11 (2021) 2003570.

5. F. Zhao, H. Zhang, R. Zhang, J. Yuan, D. He, Y. Zou, F. Gao, Emerging approaches in enhancing the efficiency and stability in non-fullerene organic solar cells, Adv. Energy Mater. 10 (2020) 2002746.
6. L. Duan, N. K. Elumalai, Y. Zhang, A. Uddin, Progress in nonfullerene acceptors, Sol. Energy Mater. Sol. Cells 193 (2019) 22-65.
7. S. Li, C. Z. Li, M. Shi, H. Chen, New phase for organic solar cell research: Emergence of Y-series electron acceptors and their perspectives, ACS Energy Lett. 5 (2020) 1554-1567.
8. W. Liu, X. Xu, J. Yuan, M. Leclerc, Y. Zou, Y. Li, Low bandgap non-fullerene acceptors enabling high performance organic solar cells, ACS Energy Lett. 6 (2021), 598-608.
9. Q. Liu, Y. Jiang, K. Jin, J. Qin, J. Xu, W. Li, J. Xiong, J. Liu, Z. Xiao, K. Sun, S. Yang, X. Zhang, L. Ding, 18 % efficiency organic solar cells, Sci. Bull. 65 (2020) 272-275
10. S. Chen, L. Feng, T. Jia, J. Jing, Z. Hu, K. Zhang, F. Huang, High-performance polymer solar cells with efficiency over 18 % enabled by asymmetric side chain engineering of non-fullerene acceptors, Sci. China Chem. 64 (2021) 1192-1199.
11. C. Zhu, L. Meng, J. Zhang, S. Qin, W. Lai, B. Qiu, J. Yuan, Y. Wan, W. Huang, Y. Li, Q Quioxaline based D-A copolymer donor achieving 17.62 % efficiency of organic solar cells, Adv. Mater. 33 (2021) 2100474.
12. J. Qin, L. Zhang. C. Zuo, Z. Xiao, Y. Yuan, S. Yang, F. Hao, M. Cheng, K. Sun, Q. Bao, Z. Bin, Z. Jin, L. Ding, A chlorinated copolymer donor demonstrates a 18.13 % power conversion efficiency, J. Semicond. 41 (2020) 10501.
13. Y. Cui, H. Yao, L. Hong, T. Zhang, Y. Tang, B. Lin, K. Xian, B. Gao, C. An, P. Bi, W. Ma, J. Hou, Organic photovoltaic cell with 17 % efficiency and superior processability, Nat. Sci. Rev. 7 (2020) 1239-1246.
14. F. Qi, K. Jiang, F. Lin, Z. Wu, H. Zhang, W. Gao, Y. Li, Z. cai, H. Y. Woo, Z. Zhu, A. K. Y. Jen. Over 17 % efficiency binary organic solar cells with photoresponse reaching 1000 nm enabled by selenophene-fused nonfullerene acceptors, ACS Energy Lett. 6 (2021) 9-15.
15. L. Liu, S. Chen, Y. Qu, X. Gao, L. Han, Z. Lin, L. Yang, W. Wang, N. Zheng, Y. Liang, Y. Tan, Nanographene–Osmapentalyne Complexes as a Cathode Interlayer in Organic Solar Cells Enhance Efficiency over 18 %, Adv. Mater. 23 (2021) 2101279.
16. M. B. Upama, Md. A. Mahmud, G. Conibeer, A. Uddin, Trendsetters in high efficiency organic solar cells: Toward 20 % power conversion efficiency, Solar RRL, 4 (2020) 1900342.

17. A. Karki, A. J. Gillett, R. H. Friend, T. Q. Nguyen, The path to 20 % power conversion efficiencies in nonfullerene acceptor organic solar cells, Adv. Energy Mater. 11 (2021) 2003441.
18. S. Lee, D. Jeong, C. Kim, C. Lee, H. Kang, H. Y. Woo, B. J. Kim, Eco-friendly polymer solar cells: Advances in green solvent processing and material design, ACS Nano 14 (2020) 14493-14527.
19. R. Xue, J. Zhang, Y. Li, Y. Li, Organic solar cell materials toward commercialization, Small 14 (2018) 1801793.
20. M. Riede, D. Spoltore, K. Leo, Organic solar cells-the path to commercial success, Adv. Energy Mater. 11 (2021) 2002653.
21. Y. Cui, L. Hong, J. Hou, Organic photovoltaic cells for indoor applications: Opportunities and challenges, ACS Appl. Mater. Interfaces, 12 (2020) 38815-38828.
22. Y. Cui, H. Yao, T. Zhang, L. Hong, B. Gao, K. Xian, J. Qin, J. Hou, 1cm^2 organic photovoltaic cells for indoor applications with over 20 % efficiency, Adv. Mater. 31 (2019) 1904512.
23. C. Zhao, J. Wang, X. Zhao, Z. Du, R. Yang, J. Tang, Recent advances, challenges and prospectus in ternary organic solar cells, Nanoscale 13 (2021) 2181-2208.
24. D. Zhou, W. You, H. Xu, Y. Tong, B. Hu, Y. Xie, L. Chen, Recent progress in ternary organic solar cells based on solution processed non-fullerene acceptors, J. Mater. Chem. A 8 (2020) 23096-23122.
25. L. Hong, H. Yao, Y. Cui, Z. Ge, J. Hou, Recent advances in high efficiency organic solar cells fabricated by eco-compatible solvents at relatively large area scale, APL Mater. 8 (2020) 120901.
26. L. Chang, M. Sheng, L. Dun, A. Uddin, Ternary organic solar cells based on non-fullerene acceptors, Org. Elect. 90 (2021) 106063.
27. P. Bi, X. Hao, Versatile ternary approach for novel organic solar cells: A review, Solar RRL, 3 (2019) 1800263.
28. X. Ma, A. Zeng, J. Gao, Z. Hu, C. Xu, J. H. Sun, S. Y. Jeong, C. Zhang, M. Li, K. Wang, H. Yan, Z. Ma, Y. Wang, H. Y. Woo, F. Zhang, Approaching 18 % efficiency of ternary organic photovoltaics with wide bandgap polymer donor and well compatible Y6; Y16-10 as acceptor, Nat. Sci. Rev. 8 (2021) nwaa305.
29. L. Zhan, S. Li, T. K. Lau, Y. Cui, X. Lu, M. Shi, C. Z. Li, H. Li, J. Hou, H. Chen, Over 17 % efficiency ternary organic solar cells enabled by two non-fullerene acceptors working in an alloy like model, Energy Environ. Sci. 13 (2020) 635-645.

30. D. Li, L. Zhu, X. Liu, W. Xiao, J. Yang, R. Ma, L. Ding, F. Liu, C. Duan, M. Fahlman, Q. Bao, Enhanced and balanced charge transport boosting ternary solar cells over 17 % efficiency, Adv. Mater. 32 (2020) 2002344.
31. J. Gao, X. Ma, C. Xu, X. Wang, j. H. Soon, S. Y. Jeong, Y. Zhang, C. Zhang. K. Wang, L. Niu, J. Zhang, F. Zhang, Over 17.7 % efficiency ternary blend organic solar cells with low energy loss and good tolerance, Chem. Engineering J. 428 (2022) 129276.
32. Q. Liu, Y. Wang, J. Fang, H. Liu, L. Zhu, X. Guo, M. Gao, Z. Tang, L. Ye, F. Liu, M. Zhang, Y. Li. Synergistically minimized nonradiative energy loss and optimized morphology achieved via the incorporation of small molecule donor in 17.7 % efficiency ternary polymer solar cells, Nano Energy, 85 (2021) 105963.
33. K. Jin, Z. Xiao, L. Ding, 18.69 % PCE from organic solar cells, J. Semicond. 42 (2021) 060502.
34. F. Liu, L. Zhou, W. Liu, Z. Zhou, Q. Yue, W. Zheng, R. Sun, W. Liu, S. Xu, H. Fan, L. Feng, Y. Yi, W. Zhang, X. Zhu, Organic solar cells with 18 % efficiency enabled by an alloy acceptor: A two in one strategy, Adv. Mater. 33 (2021) 2100830.
35. Y. Jiang, X. Zhu, High performance ternary organic solar cells enabled by synergizing fullerene and non-fullerene acceptors, Org. Mater. 3 (2021) 254-276.
36. Y. Zhang, G. Li. Functional third components in nonfullerene acceptor based ternary organic solar cells, Acc. Mater. Res. 1 (2020) 158-171.
37. Y. Xie, F. Yang, Y. Li, M. A. Uddin, P. Bi, B. Fan, Y. Cai, X. Hao, H. Y. Woo, W. Li, F. Liu, Y. Sun, Morphology control enables efficient ternary organic solar cells, Adv. Mater. 30 (2018) 1803045.
38. J. Feng, H. Wang, N. Rujisamphan, Y. Li, Theoretical design of dithienopicenocarbazole -based molecules by molecular engineering of terminal units towards promising non-fullerene acceptors, Front. Chem. 8 (2020) 580252.
39. Pierre D. Harvey, Ganesh D. Sharma, Bernhard Witulski, Indolo- and Diindolocarbazoles in Organic Photovoltaic Cells, Chem. Lett. 50 (2021) 1345-1355.
40. H. Wang, Z. Zhang, J. Yu, X. Liu, S. Qu, S. Guang, W. Tang, Nonacyclic carbazole based nonfullerene acceptors enable over 12 % efficiency with enhanced stability for organic solar cells, J. Mater. Chem. A 7 (2019) 21903-21910.
41. Y. T. Hsiao, C. H. Li, S. L. Chang, S. Heo, K. Tajima, Y. J. Cheng, C. S. Hsu. Haptacyclic carbazole based ladder type nonfullerene acceptor with side chain optimization for efficient organic photovoltaics, ACS Appl. Mater. Interfaces 9 (2017) 42035-42042.

42. W. Guo, B. Zhao, J. Xin, H. Liu, Y. Mi, J. Zhang, Z. Guo, W. Wei, W. Ma, C. Gao, Z. An. Nonfullerene small molecular acceptors based on dithienocyclopentafluorene and dithienocyclopentacarbazole cores for polymer solar cells, Dyes and Pigments 144 (2017) 48-57
43. Q. Cao, W. Xiong, H. Chen, G. Cai, G. Wang, L. Zheng, Y. Sun. Design, synthesis, and structural characterization of the first dithienocyclopentacarbazoe based n-type organic semiconductor and its application in non-fullerene polymer solar cells, J. Mater. Chem. A 5 (2017) 7451-7461.
44. T. W. Chen, J. Y. Yu, Y. W. Lin, S. H. Peng, S. H. Wu, Y. J. Su, V. K. Karapala, L. Hong, H. Yao, J. Hou, C. s. Hsu, Chlorinated carbon bridged and silicon carbazole based nonfullerene acceptors manifest synergistic enhancement in ternary organic solar cell with efficiency over 15 %, Solar RRL 4 (2020) 2000357.
45. Q. He, M. Zhahid, X. Jiao, E. Gann, F. D. Eisner, T. Wu, Z. Fie, T. D. Anthopoulos, C. R. McNeill. M. Heeney, Crucial role of fluorine in fully alkylated ladder type carbazole based nonfullerene organic solar cells, ACS Appl. Mater. interfaces 12 (2020) 9555-9562.
46. S. L. Chang, K. E. Hung, F. Y. Cao, K. H. Huang, C. S. Hsu, C. Y. Liao, C. H. Lee, Y. J. Cheng, Isomerically pure benzothiophene incorporated acceptor : achieving improved Voc and Jsc of nonfullerene organic solar cells via end group manipulation, ACS Appl. Mater. Interfaces 11 (2019) 33179-33187.
47. Q. Tu, Y. Ma, X. Zhou, W. Ma, Q. Zheng. Enhancing the photovoltaic performance of ladder type dithienocyclopentacarbole based nonfullerene acceptors through fluorination and side chain engineering, Chem. Mater. 31 (2019) 5953-5963.
48. L. Tanguy, P. Malhotra, S. P. Singh, G. Brisard, G. D. Sharma, P. D. Harvey. A 91.6 % power conversion efficiency organic solar cell with a porphyrin conjugated polymer using a nonfullerene acceptor, ACS App. Mater. Interfaces 11 (2019) 28078-28087.
49. Suman, A. Siddiqui, M. L. Keshtov, G. D. Sharma, S. P. Singh. New indolo carbazole based nonfullerene n-type semiconductors for organic solar cell applications, J. Mater. Chem. C 7 (2019) 543-552.
50. L. Bucher, N. Desbois, P. D. Harvey, C. P. Gros, R. Misra, G. D. Sharma, Nonfullerene polymer solar cells reaching a 9.29 % efficiency using a BOUIPY thiophene backboned donor materials, ACS Appl. Energy Mater. 1 (2018) 3359-3368.

51. Y. Jia, S. C. Huang, T. W. Chen, L. C. Chueh, Y. Cui, L. Hong, H. Yao. Elucidating end group modifications of carbazole based nonfullerene acceptors in indoor applications for achieving a PCE of over 20 %, ACS Appl. Mater. Interfaces 13 (2021) 2647-26255.
52. T. W. Chen, V. K. Karapala, J. T. Chen, C. S. Hsu, Recent advances of carbazole based nonfullerene acceptors: Molecular design, optoelectronic properties, and photovoltaic performance in organic solar cells, J. Chinese Chem. Soc. 68 (2021) 1186-1196.
53. A. Singh, C. K. Lim, Y. D. Lee, J. H. Maeng, S. Lee, J. Koh, S. Kim. Tuning solid state fluorescence to the near infrared : a combinational approach to discovering molecular nanoprobes to biomedical imaging, ACS Appl. Mater. Interfaces 5 (2013) 8881-8888.
54. A. N. Krol, R. Wagener, F. Kraus, A. Mishra, P. Bauerle, F. Wurthner, Modulation of bandgap and p- versus n -semiconductor character of ADA dyes by core and acceptor group variation, Org. Chem. Front. 3 (2016) 545-555.
55. T. Kono, Y. Shibata, Z. Wang, T. Miyader, Y. Yoshida, Synthesis of novel push-pull chromophores based on N-ethylcarbazole for vacuum deposition processed organic photovoltaics, Chem. Lett. 44 (2015) 958-960.
56. A. Carella, R. Centore, F. Borbone, M. Toscanesi, M. Trifuoggi, F. Bella, C. Gerbaldi, S. Galliano, E. Schiavo, A. Massaro, A. B. Munoz-Garcia, M. Povone, Tuning optical and electronic properties in novel carbazole photosensitizers for p-type dye sensitized solar cells, Electrochimica Acta, 292 (2018) 805-816.
57. M. L. Keshtov, S. A. Kuklin, I. O. Konstantinov, A. R. Khokhlov, Z. Xie, C. Dou, E. N. Koukaras, R. Suthar, G. D. Sharma, Synthesis and photovoltaic properties of new conjugated D-A polymrs based on same fluoro-benzothiadiazole acceptor unit and different donor units, ChemistrySelect 5 (2020) 853-863.
58. S. Chen, Y. Wang, L. Zhang, J. Zhao, Y. Chen, D. Zhu, H. Yao, G. Zhang, W. Ma, R. H. Friend, P.C. Y. Chow, F. Gao, H. Yan. Efficient nonfullerene organic solar cells with small driving forces for both hole and electron transfer, Adv. Mater. 30 (2018) 1804215.
59. N. K. Elumalai, A. Uddin, Open circuit voltage of organic solar cells : an in-depth review, Energy Environ. Sci. 9 (2016) 391-410.
60. Y. He, Y. Li, Fullerene derivative acceptors for high polymer solar cells, Phys. Chem. Chem. Phys. 13 (2011) 1970-1983.

61. M. Zhang, Z. Xiao, W. Gao, Q. Liu, K. Jin, W. Wang, Y. Mi, Q. An, X. Ma, X. Liu, C. Yang, L. Ding, F. Zhang, Over 13 % efficiency ternary nonfullerene polymer solar cells with titled up absorption edge by incorporating a medium bandgap acceptor, Adv. Energy Mater. 8, 1801968, 2018
62. C. Xu, K. Jin, Z. Xiao, Z. Zhao, X. Ma, X. Wang, J. Li, W. Xu, S. Zhang, L, Ding, F. Zhang, Wide bandgap polymer with narrow photon harvesting in visible range enables efficient semitransparent organic photovoltaics, Adv. Funct. Mater. doi: 10.1002/adfm.202107934
63. X. Ma, J. Wang, Q. An, J. Gao, Z. Hu, C. Xu, X. Zhang, Z. Liu, F. Zhang, Highly efficient quaternary organic photovoltaics by optimizing photogenerated exciton distribution and active layer morphology, Nano Energy 20, 104496 (2020)
64. X. Wang, Q. Sun, J. Gao, X. Ma, J. H. Son, S. Y. Jeong, Z. Hu, L. Niu, H. Y. Woo, J. Zhang, F. Zhang, Ternary organic photovoltaics cells exhibiting 17.59 % efficiency with two compatible Y6 derivatives as acceptor, Solar RRL 5, 2100007 (2021)
65. Liu X, Yan Y, Honarfar A, Yao Y, Zheng K, Liang Z. Unveiling excitonic dynamics in high efficiency nonfullerene organic solar cells to direct morphological optimization for suppressing charge recombination, Adv Sci. 6 (2019) 1802103.
66. Zhang G, Zhang K, Yin Q, Jiang X-F, Wang Z, Xin J, Ma W, Yan H, Huang F, Cao Y. High-performance ternary organic solar cell enabled by a thick active layer containing a liquid crystalline small molecule donor, J Am Chem Soc. 139 (2017) 2387–2395.
67. Kyaw AKK, Wang DH, Gupta V, Leong WL, Ke L, Bazan GC, Heeger AJ. Intensity dependence of current-voltage characteristics and recombination in high-efficiency solution-processed small-molecule solar cells, ACS Nano 7 (2013) 4569–457.
68. Kirchartz T, Deledalle F, Tuladhar PS, Durrant JR, Nelson J. On the differences between dark and light ideality factor in polymer:fullerene solar cells, J. Phys. Chem. Lett. 4 (2013) 2371–2376.
69. X. Ma, Q. An, O. A. Ibraikulov, P. Leveque, T. Heiser, N. Leclerc, X. Zhang, F. Zhang, Efficient ternary organic photovoltaics with two polymer donors by minimizing energy loss, J. Mater. Chem. A 8 (2020), 1265-1272.

70. J. Gao, J. Wang, Q. An, X. Ma, Z. Hu, C. Xu, X. Zhang, F. Zhang, Over 16.7 % efficiency of ternary organic photovoltaics by employing extra PC71BM as morphology regulator, Sci. China Chem. 63 (2020) 83-91.
71. Wang Y, Qian D, Cui Y, Zhang H, Hou J, Vandewal K, Kirchartz T, Gao F. Optical gaps of organic solar cells as a reference for comparing voltage losses, Adv. Energy Mater. 8 (2018) 1801352.
72. Wang H, Zhang Z, Yu J, Lin P-C, Chueh C-C, Liu X, Guang S, Qu S, Tang W. Over 15% efficiency in ternary organic solar cells by enhanced charge transport and reduced energy loss, ACS Appl. Mater. Interfaces 12 (2020) 21633-40.
73. B. Qiu, S. Chen, C. Sun, J. Yuan, X. Zhang, C. Zhu, S. Qin, L. Meng, Y. Zhang, C. Yank, Y. Zou, Y. Li, Understanding the effect of the third component $PC_{71}BM$ on nanoscale morphology and photovoltaic properties of ternary organic solar cells, Solar RRL 4 (2020) 1900540.